CHAPTER III
EXPERIMENTAL

3.1 Materials

High density polyethylene and polystyrene (suppliers and grades given in Table 3.1) were used as matrix and droplet phases, respectively. Both polystyrene grades were obtained from the manufacturers in the form of flake; they were crushed and size-selected by passing the flakes through a 425-mm sieve. To eliminate volatile components, all polymers were heated to around 80°C under vacuum for 12 hours. The polymer blend systems and their experimental temperature are shown in Table 3.2.

Table 3.1 Properties of polymer blend components

Polymer	Suppliers	Grade	M_w*	Melt Flow Index (g/10min)
PS1	Polyscience	Cat#18544	50,000	-
PS2	Polyscience	Cat#23637	800-5,000	-
HDPE1	Bangkok Polyethylene	1600J	-	14
HDPE2	Aldrich	Cat#42,801-9	-	42

* Quoted by the manufacturers

Table 3.2 Polymer blend systems

Blend system	Blend components (Drop/Matrix)	Temperature (°C)
A	PS1/HDPE1	147
B	PS2/HDPE2	139

3.2 Rheological Characterization

Each polymer was molded into a disk, 25 mm in diameter and 1 mm thick by using a compression mold (Wabash, model V50H-18-CX) at 145°C for HDPE1 and PS1, and at 135°C for HDPE2 and PS2 under a force of 10 tons. We used a cone-and-plate rheometer (Rheometrics Scientific: Model ARES, 25-mm plate diameter with cone angle 0.1 rad) to obtain viscosities and first normal stress differences of the pure polymers. From the rheological properties of pure polymers at various temperatures, the desired pairs of polymers and operating temperatures were selected for further study; and their steady-state viscosities and first normal stress differences as functions of shear rate are shown in Fig. 3.1 (a) and (b). At low shear rates, the ratio of droplet-to-matrix first normal stress differences N_{1r} of system B could not be precisely determined due to the force-measurement limitations of the rheometer. However, in the low-shear-rate and low-frequency regimes, $N_1(\dot{\gamma})$ is approximately equal to twice G' (ω) at $\dot{\gamma}=\omega$, thus N_{1r} can be estimated by the corresponding ratio of storage moduli, G'_r. The viscosity ratios and G' ratios of the two polymer systems are shown in Fig. 3.2. In addition, the stabilities of all polymers to thermal degradation were tested at their experimental temperatures by measuring the viscosity at a constant shear rate, 0.5 s^{-1}, for 4 hours; in all cases the viscosity values remain unchanged, allowing us to conduct blend experiments on each system for periods as long as four hours.

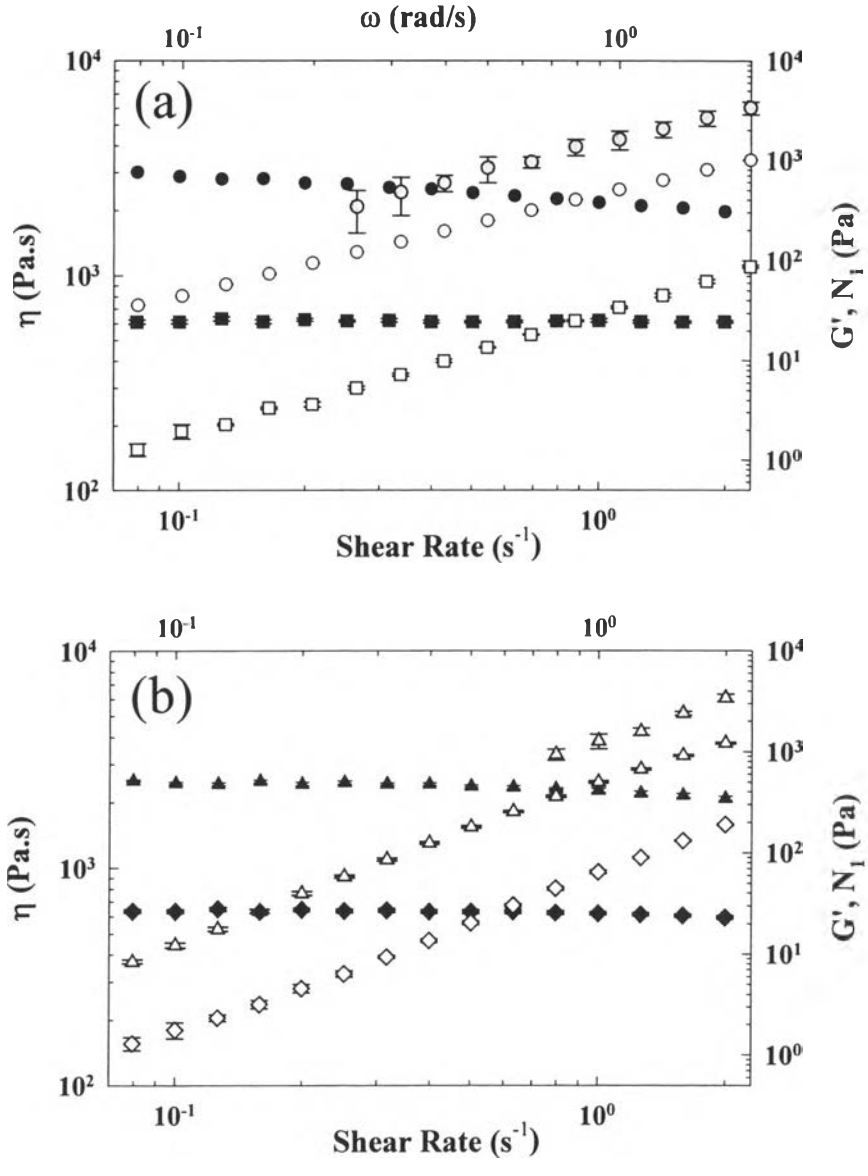

Figure 3.1 Viscosity η, storage modulus G', and first normal stress difference N_1 as functions of shear rate and frequency for each pure polymer at the temperatures at which the blend experiments were carried out; (a) matrix phase [HDPE1 at 147°C: η (●), G' (o), and N_1 (○), HDPE2 at 139°C: η (■) and G'(□)] and (b) droplet phase [PS1 at 147°C: η (▲), G' (△), and N_1 (△), PS2 at 139°C: η (◆) and G'(◇)].

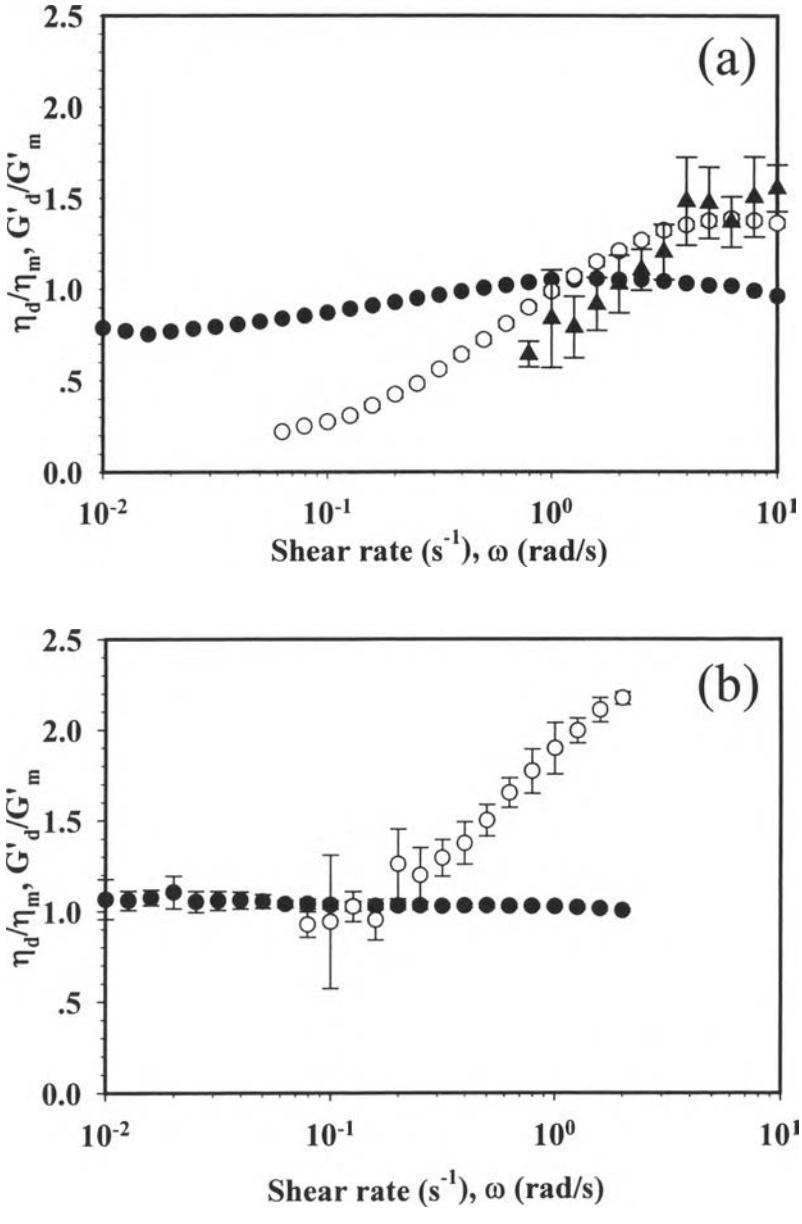

Figure 3.2 The ratios of droplet to matrix values of the viscosity η (●), storage modulus G' (o), and first normal stress difference N_1 (▲) for (a) system A: PS1/HDPE1 at 147°C and (b) system B: PS2/HDPE2 at 139°C. These two temperatures apply to all results in the following figures for systems A and B, respectively.

3.3 Observations of an Isolated Droplet in Shearing Flow

3.3.1 Shearing Apparatus

To observe the droplet behaviors in simple shearing flow, we used a flow cell (Linkam CSS 450, Linkam Scientific Instruments Ltd., UK) consisting of two transparent quartz parallel disks mounted on an optical microscope (Leica DMRPX, Leica Imaging Systems LTd., Cambridge, England), and connected to a CCD camera (Cohu 4910, Cohu Inc., CA). In addition, the images were analyzed on a computer using the Scion image software.

3.3.2 Sample Preparation

HDPE used as the matrix polymer was molded into a disk 25-mm in diameter and 0.5-1 mm thick by compression molding at 145°C for HDPE1 and 135°C for HDPE2. Various PS droplets were introduced into the matrix by using a pin to put a small amount of PS powder on a HDPE disk, and then covering this with another HDPE disk to form a sandwich. The sample was then placed between the top and the bottom disks of the flow cell, both of which were brought into contact with the sample, which was then heated to the testing temperature.

3.3.3 Determination of Interfacial Tension

We attempted to determine the interfacial tensions by measuring the deformation parameter Def (cf. Eq. 1.2) of a retracting droplet vs. time, which is known to decay exponentially [Lucinia *et al.* (1997)]:

$$Def = Def_o \exp\left(-\frac{t}{\tau}\right) \tag{3.1}$$

so that the slope of Def vs. t on a semi-log plot can be related the characteristic relaxation time for a single drop, τ. By equating this characteristic relaxation time to that predicted by the Palierne model (Eq. 3.2) [Palierne (1990) and Graebling *et al.* (1993)], the interfacial tension was then calculated from the following relation

$$\tau = \frac{(3 + 2\eta_r)(16 + 19\eta_r) r_o \eta_{m,o}}{40(1 + \eta_r)\Gamma} \tag{3.2}$$

To obtain images of the relaxing droplet after a large strain, the desired strain was imposed onto a selected drop in the field of view of the microscope which moved the droplet out of the field of view, then the droplet was left to relax at least 40-50 min (which is equal to or greater than the droplet relaxation time) to ensure that the drop had returned to the spherical shape, and then the droplet was moved back into the field of view by imposing the same strain in the reverse direction. A hundred to 200 images were then recorded (10-20 second per frame) while the droplet relaxed its shape. For both systems, the droplet size was varied from around a hundred micron up to 400 μm or thereabouts. Fig. 3.3 (a) and (b) shows that the apparent interfacial tension values inferred from Eq. 3.2 increases with the droplet size. This dependence of apparent interfacial tension on droplet size is likely caused by the contribution of droplet elasticity to the relaxation of the droplet shape. For large enough droplets, relaxation should become slow enough that viscoelastic stresses relax too quickly to influence droplet shape relaxation and hence the rate of relaxation is governed by interfacial tension alone. Thus, the interfacial tension value obtained for large droplets is expected to be the most accurate. Unfortunately, because of the limitation in the ratio of a gap width to an initial droplet size, which was kept at greater than 5, we cannot attain a regime in which the apparent interfacial tension becomes independent of droplet size; see Fig. 3.3. Therefore, the values of the interfacial tension for the polymer blend systems used in this work were taken from the literature [Brandrup and Immergut (1989)], which are 5.79 mN/m for system A at 147°C, and 5.92 mN/m for system B at 139°C.

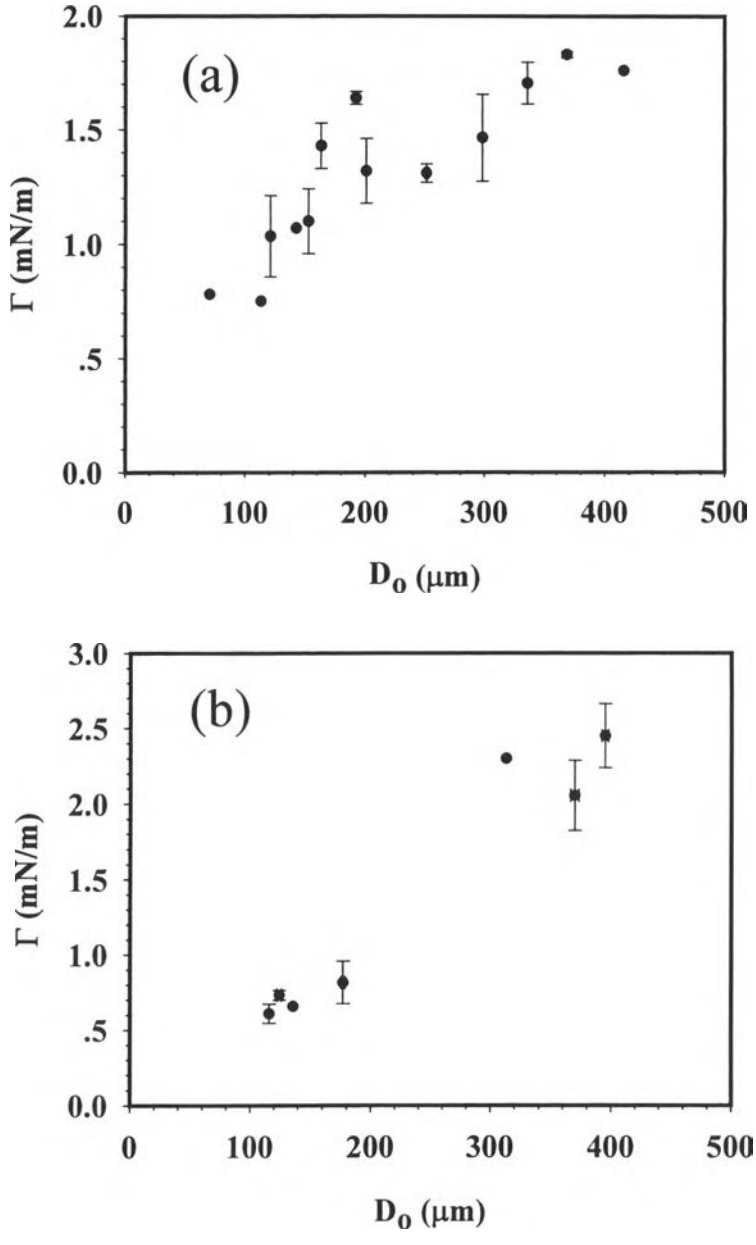

Figure 3.3 Dependence of apparent interfacial tension value on droplet size for (a) system A and (b) system B, inferred from the Palierne formula, Eq. 3.2.

From the optical microscope, the droplet images were captured only from the top view, i.e., a view containing the flow and vorticity directions. Since only a projection of the droplet onto the vorticity plane can be imaged from this view, this view cannot determine the true lengths of the principal axes, because two of them (those in the flow and the shear-gradient directions) are not parallel to the

vorticity plane. However, the lengths of these axes can be determined by using the affine angle of rotation of the droplet in the plane containing the flow and shear-gradient directions (Larson 1988) together with the condition of volume preservation, $D_o^3 = abc$ (Almusallam *et al.* 2000).

Although the lengths of the principal axes can be approximated by using the method mentioned above, for convenience the lengths of the observable axes, shown in Fig. 3.4, were used here to describe the behavior of each droplet by defining a modified deformation parameter Def* as:

$$Def^* \equiv \frac{a^* - c}{a^* + c} \tag{3.3}$$

where the asterisk denotes that the deformation parameter is an apparent one obtained from the droplet image projected into the flow-vorticity plane; see Fig. 3.4.

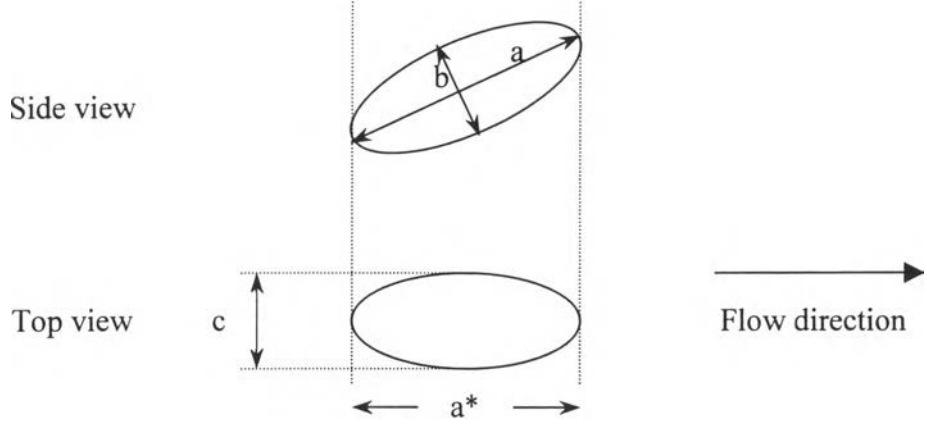

Figure 3.4 Schematic drawing of a single drop observed from the "side" and "top" view by optical microscopy, a and b: the long and short axes of the droplet in the flow-gradient plane, a*: the a axis projected into the flow direction and c: the principal axis in the radial direction.

3.3.4 Transient Deformation

The deformed shapes were observed as a function of time from initial to steady-state shapes. Because the Linkham device has one stationary and one moving plate, a single droplet cannot be viewed continuously from startup of shearing to steady-state shape, since this droplet will pass out of the viewing plane after imposition of around 10 strain units. However, since the behavior of a given isolated droplet is highly reproducible, the strain dependence of the deformation can be determined by combining the results of several experiments. In experiments of type 1, we first move the droplet out of the viewing window by imposing a shearing strain of less than 40 strain units. After allowing the droplet to relax its shape for at least 40 minutes, an observed shear rate was imposed at the same strain but in opposite direction, eventually bringing the droplet back into the viewing window, where it could be observed during deformation. However, the droplet could not be subjected to a large strain in this type of experiment, since this would move the droplet again out of the viewing window. So, to obtain droplet deformation at large strains, we performed experiments of type 2, in which we sheared continuously, and imaged the droplet each time it passed through the viewing window in its orbit around the device. Typically, one orbit would require around 40 strain units. To get a clear image of the droplet without a high-speed camera, we stopped the flow briefly each time the droplet reached the center of the viewing image and video recorded its shape over a period of around 1 second, which is a time much too short for the droplet to relax its shape significantly. Then the flow was resumed again until the droplet again reached the viewing window. By repeating the experiment on droplets of similar size, which were stopped at different times, we could assemble a consistent curve from multiple droplets of the droplet deformation versus time at a given shear rate. In the following, the results from different droplets will be presented using different symbols, showing the consistency of results combined from multiple droplets. In each experiment, the time for one revolution of a droplet was recorded with a stopwatch along with the time shown on the Linksys program. To avoid interactions with the plates, the ratio of the gap width to the initial diameter of a selected drop was kept higher than 10, and only droplets near the center of the gap were observed. The experiment was repeated with more than 10 droplets with initial

diameters around 75 (±10%) μm. were used, and the imposed shear rate was 0.5 s^{-1}. Similar experiments (only type 2) were carried out using other droplet sizes, 52, 110 and 120 μm, but the same shear rate of 0.5 s^{-1}. To separate the effect of shear rate from that of elasticity, another set of experiments were carried out on droplets of different sizes [135, 75, and 46 μm] but in which the shear rate varied inversely with droplet size from 0.28, to 0.5, to 0.8 s^{-1}, In this way we could vary the viscoelastic forces, which increase with increasing shear rate, while holding the capillary number fixed at around 25 by varying the droplet size inversely with the shear rate.

3.3.5 Steady-State Deformation and Breakup

From the transient experiments, the required strain to reach steady state can be determined and was found to be around 2500 strain units. To determine the steady-state droplet shape as a function of capillary number, we carried out experiments up to high strains at two different shear rates and for different droplet sizes. The selected shear rates were 0.3 and 0.5 s^{-1} for system A, and 1 s^{-1} for system B, which are high enough that the needed strain could be achieved within an acceptable time, but not so high that the droplet moves too fast to be observed. At a higher shear rate, droplet sizes that would be attainable a steady state shape are too small to be effectively observed. In addition to using these two shear rates, Different droplet sizes were chosen to vary the capillary number at fixed elasticity. After loading a sample, droplets were allowed to relax to spherical shapes for a period of at least 50 minutes, a bit longer than for the transient experiments described earlier, since some of the droplets used were larger and so needed somewhat longer to relax. A constant shear rate was then applied until a strain exceeding 2500 strain units had accumulated. When a selected droplet passed through the viewing window, the motor was stopped for less than a second and a video movie (speed 25-fps) was then recorded, as described earlier in the description of the experiments measuring transient droplet shapes. To ensure that the steady state deformation had indeed been attained, we repeated imaging the same droplet for several more passes of the droplet through the viewing window over a period of 5 to 10 min. In addition, after turning

off the flow the droplet shape relaxation was recorded at a video recording speed of 10-20 seconds per frame for approximately 1 hour.

When the droplet size was varied at fixed shearing rate, we found a critical droplet size above which no steady state-shape was obtained. For these droplets, the unstable shape of the droplet was recorded with time, by imaging the droplet each time it passed through the viewing window (as in the experiments discussed earlier), until the droplet broke.